

Article

The Microstructural Characterization and Mechanical Properties of 5 vol. % (TiB_w + TiC_p)/Ti Composite Produced by Open-Die Forging

Jianchao Han ¹, Zhidan Lü ², Changjiang Zhang ^{2,*}, Shuzhi Zhang ² , Hongzhou Zhang ³, Peng Lin ² and Peng Cao ^{3,*} 

¹ School of Mechanical Engineering, Taiyuan University of Technology, Taiyuan 030024, China; hanjianchao@tyut.edu.cn

² School of Materials Science and Engineering, Taiyuan University of Technology, Taiyuan 030024, China; zdLv_tyut@163.com (Z.L.); zhshzh1984@163.com (S.Z.); linpeng@tyut.edu.cn (P.L.)

³ Department of Chemical and Materials Engineering, University of Auckland, Private Bag 92019, Auckland 1142, New Zealand; hzha243@aucklanduni.ac.nz

* Correspondence: zhangchangjiang@tyut.edu.cn (C.Z.); p.cao@auckland.ac.nz (P.C.); Tel.: +86-351-6010022 (C.Z.); +64-9-923-6924 (P.C.)

Received: 25 May 2018; Accepted: 22 June 2018; Published: 25 June 2018



Abstract: In this study, a Ti composite reinforced with 5 vol. % (TiB_w + TiC_p) was fabricated by an in situ casting route. Open die forging in (α + β) phase region was conducted on the composite casting. The microstructures of the as-forged composite pancake are inhomogeneous in terms of matrix microstructure and distribution of reinforcements. The matrix grains are gradually refined from the periphery to centre of the pancake. The reinforcements TiB_w and TiC_p tend to be uniformly distributed in the centre region. It is suggested that the microstructure difference can be mainly ascribed to the temperature variation from the periphery to the centre. The tensile testing results show that the centre region of the composite pancake exhibits higher strength than the peripheral region. The mechanical behaviour of the composite pancake with the temperature is discussed.

Keywords: titanium matrix composites; in situ formed reinforcements; microstructure; mechanical properties; forging

1. Introduction

Due to the high elastic modulus, specific strength, superior creep and fatigue resistances, titanium matrix composites (TMCs) have been emerged as attractive candidate materials for high-temperature structural applications in aerospace and automotive industries [1–4]. As one approach for producing TMCs, in situ synthesis techniques have drawn extensive interest because of their superior properties along with the ease of fabrication [5–7]. Among the reinforcements available for TMCs, TiB whiskers (TiB_w) and TiC particles (TiC_p) are the most suitable reinforcements since they possess high thermal stability, similar density and thermal expansion coefficient to titanium alloys, high modulus and stiffness [8–10]. In recent years, several new processing techniques for synthesizing titanium MMCs have been developed; in particular, additive manufacturing has attracted increasing interest [11,12]. Some new titanium alloy MMCs are also being developed such as Ti-MMCs with carbon-based reinforcements [13].

It is noted that, along with the limited improvement in strength, the in situ TiB_w/Ti or TiC_p/Ti composites prepared by in situ casting routes demonstrate very low room-temperature ductility and poor temperature resistance, which is inadmissible for structural materials [14,15]. Hot working of the TMCs is usually used to refine the microstructure and improve the distribution of reinforcements [16,17].

However, $(\text{TiB}_w + \text{TiC}_p)/\text{Ti}$ composites are more difficult to process, as compared with the titanium alloys with minor boron or carbon addition. According to previous studies by Bhat et al. [18] and Liu et al. [19], the non-uniform deformation microstructure and the crack of reinforcements are commonly observed because of the existing temperature variation and the mismatched deformation between the reinforcement and the matrix during hot deformation. The non-uniform microstructure and reinforcement cracking will induce deformation incompatibility and flow localization during subsequent forming process and deteriorate the mechanical properties of final products. Therefore, how to ensure homogeneous deformation microstructure and reduce the microvoids is of significant importance and needs to be considered during the processing of $(\text{TiB}_w + \text{TiC}_p)/\text{Ti}$ composites. In fact, research on the non-uniform deformation microstructures of Ti alloy [20] and TiAl [21] has been conducted. However, there are no systematic studies available on the microstructural homogeneity and the relative tensile properties of TiB_w/Ti or TiC_p/Ti composites during thermomechanical processing.

In this paper, 5 vol. % $(\text{TiB}_w + \text{TiC}_p)/\text{Ti}$ composite was in situ synthesised via a casting route, followed by open die forging in $(\alpha + \beta)$ phase region. The main objective is to investigate microstructural characteristics and tensile properties of the composite samples taken from different sampling points.

2. Materials and Methods

The materials used in the experiment was a near- α high-temperature titanium alloy (Ti-6Al-2.5Sn-4Zr-0.7Mo-0.3Si) reinforced with 5 vol. % $(\text{TiB}_w + \text{TiC}_p)$ reinforcements (TiB:TiC = 1:1). The raw materials for preparing the composite were grade I sponge titanium (99.9%), B_4C powder (98%), graphite powder and other alloying elements, including Al (99.99%), Sn (99.9%), sponge Zr (99.9%), crystal Si (99.9%) and Al-Mo master alloy. The raw materials were melted in an induction skull melting furnace (ISM) and the detailed procedure was described in our previous study [5]. The β transus temperature of the composite verified by differential scanning calorimetry (DSC) is approximately 1105 °C. A cylindrical billet (Φ 130 mm \times 150 mm) was cut from the composite ingot by electric discharge machining (EDM). Then the billet was subjected to open die forging using a hydraulic press at 1050 °C with a strain rate of 0.01 s⁻¹ followed by air cooling (the forging process is shown in Figure 1a). Prior to forging, the billet was preheated for 0.5–1 h in a resistance furnace and then forged with a total deformation of 75%. Finally, a forged pancake with a diameter of 260 mm and a thickness of 37 mm was obtained without macroscopic cracks (Figure 1b). The composite pancake was cut by EDM for microstructural observation and tensile test. The four sampling points of the as forged composite pancake from periphery to centre are shown in Figure 1c.

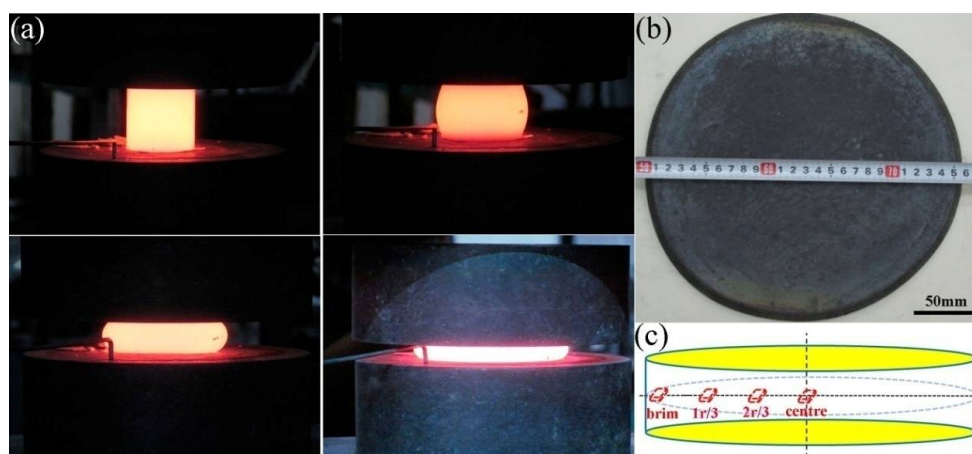


Figure 1. Preparation of the as forged composite pancake: (a) forging process; (b) macrograph of composite pancake; (c) schematic diagram showing the sampling points taken from the composite pancake.

The microstructures were characterised by an FEI-Quanta-200F scanning electron microscope (SEM, FEI, Hillsboro, OR, USA) equipped with electron back scattered diffraction (EBSD, EDAX, Mahwah, NJ, USA) and a Philips-CM12 transmission electron microscope (TEM, Philips, Amsterdam, Netherlands). The image analysis software Image-Pro Plus (ver 6.0, Media Cybernetics, Rockville, MD, USA) was used to investigate the characteristics of the reinforcements and the matrix microstructure. All examinations were performed on the cross-sections parallel to the forging direction. Flat dog-bone-shaped tensile specimens (Figure 2) were cut from the four locations (from peripheral to central regions) of the composite pancake, as shown in Figure 1c. Tensile tests were carried out on an INSTRON-5500R testing machine (Instron, Boston, MA, USA) at 25 °C, 600 °C, 650 °C and 700 °C, with a constant displacement rate of $8.3 \times 10^{-3} \text{ mm}\cdot\text{s}^{-1}$. For all of these tensile tests, at least three tensile samples were tested to report an average value. The fracture surfaces were observed by SEM after tensile tests to investigate the fracture mechanism.

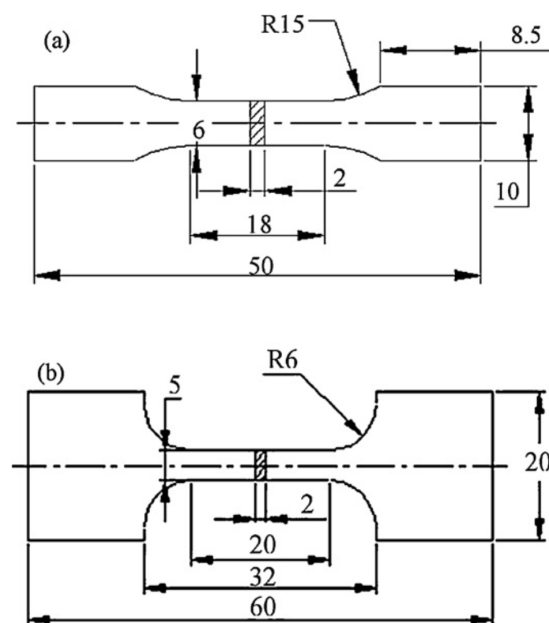


Figure 2. Dimensioned schematic of the tensile specimen: (a) room temperature specimen; (b) high temperature specimen. Note: all dimensions are in mm.

3. Results and Discussion

3.1. Microstructure

As reported in our previous study [5], the phases formed in the composite are TiB, TiC, α -Ti and β -Ti. Figure 3 shows the deformation microstructure at different sampling points within the as-forged (TiB_w + TiC_p)/Ti composite. In terms of the reinforcements, the dominating feature in the peripheral region is the crack of TiB_w and TiC_p with nearly random distribution. Moreover, the microvoids are usually observed near the tips of the reinforcements, as shown in Figure 3a. In the samples taken from (1/3)r and (2/3)r to the centre (see Figure 1c), the TiB_w and TiC_p are more or less aligned perpendicular to the forging direction. In addition, it is worth mentioning that the cracking of the reinforcements occurs more frequently at the TiB_w whiskers with high aspect ratio rather than at nearly equiaxed TiC_p particles. The spaces between the fractured TiB_w are filled with matrix leaving no noticeable voids, as shown in Figure 3b–d. Different matrix microstructures were observed at different sampling points. As shown in Figure 3a, the microstructure of the peripheral region is composed of nearly equiaxed α grains and transformed β grains, which does not have any deformation characteristics. Unlike the results shown in Figure 3a, some coarse and elongated primary α grains appear in Figure 3b, which

means that the dynamic recrystallization (DRX) did not proceed completely at the sampling points of one third r . From Figure 3c,d, it can be clearly seen that the microstructures at the sampling points of two thirds r and the centre area are characterised by dominant fine DRX grains, in addition to few transformed β grains.

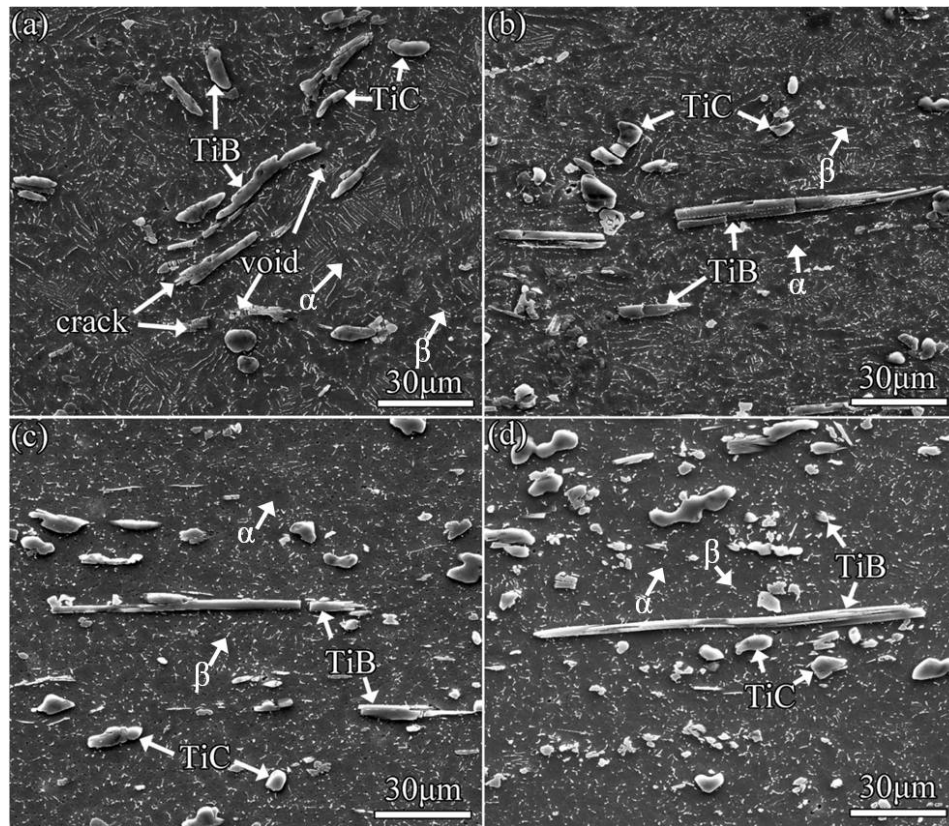


Figure 3. Microstructure homogeneity analysis of the as-forged composite pancake. Sample was cut at: (a) near periphery; (b) $(1/3)r$ to the periphery; (c) $(2/3)r$ to the periphery; (d) near centre (i.e., r to the periphery).

The TEM images in Figure 4 reveals the matrix microstructures of the $(TiB_w + TiC_p)/Ti$ composite pancake. In the peripheral region, the predominant feature in the matrix microstructure is the fine α subgrains. Each α subgrain is surrounded by adjacent α subgrains, as shown in Figure 4a. In addition, it can be seen from Figure 4b that some α subgrains contain a large number of dislocations. The α subgrains are generally induced by dislocation recovery due to the high stored energy generated during forging. In contrast, in the centre area, some fine equiaxed DRX α grains can be clearly seen and the dislocations density appears to be much lower, as shown in Figure 4c,d.

According to Figures 3 and 4, the dynamic recrystallisation mainly occurs in the centre region during forging. Therefore, EBSD was used to further characterise the matrix microstructure in the centre area. Figure 5a is the inverse pole figure (IPF) map, in which different colour codes indicate the different crystal orientation. No obvious texture characteristic exists in the centre area of the composite pancake. Figure 5b presents the grain boundary map overlaid with low ($2^\circ \leq \theta \leq 15^\circ$) and high ($\theta \geq 15^\circ$) angle boundaries. The low-angle grain boundaries ($2^\circ \leq \theta \leq 15^\circ$) described by red and green lines amount for 35.7%, while the high-angle grain boundaries ($\theta \geq 15^\circ$) depicted by blue lines occupy 64.3%. Thus, the matrix microstructure is characterised by predominant fine equiaxed DRX grains with some refined subgrains. It is well documented that high angle boundaries are generally caused by dynamic recrystallization and grain growth, while low angle boundaries are normally the features of substructures generated in the recovery stage. The distribution of the DRX grain size is shown in

Figure 5c. Overall, the DRX grain size is $<7\ \mu\text{m}$, the majority of grains (80% grains) are below $4\ \mu\text{m}$. Very limited numbers of DRX grains grow to a size $>7\ \mu\text{m}$, while 23.2% of grains or subgrains are smaller than $2\ \mu\text{m}$. Thus, the coarse casting matrix microstructure of the composite has been effectively broken down by dynamic recrystallization during forging.

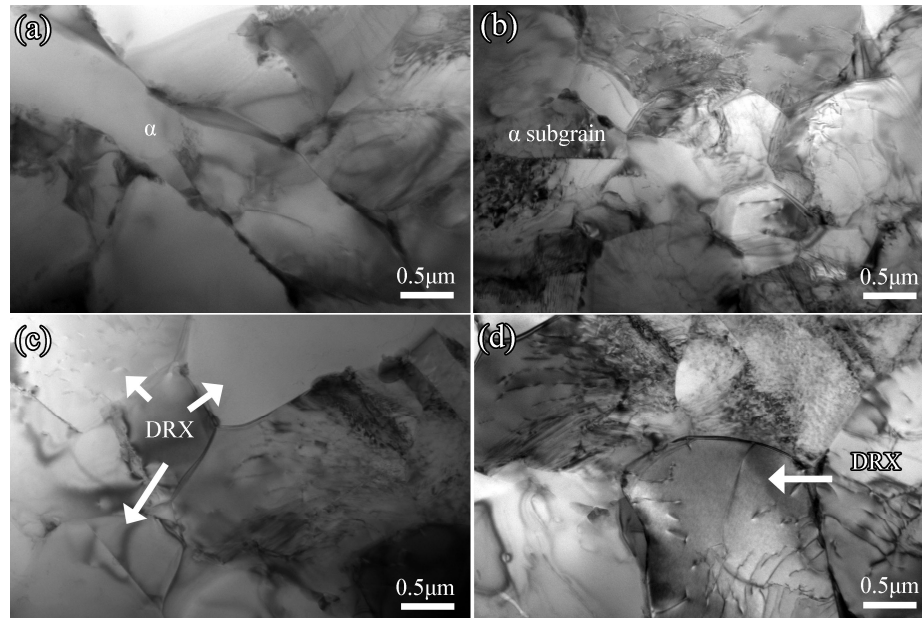


Figure 4. TEM micrographs presenting the matrix microstructure of the $(\text{TiB}_w + \text{TiC}_p)/\text{Ti}$ composite pancake in different sampling points: (a,b) near the periphery; (c,d) near the centre.

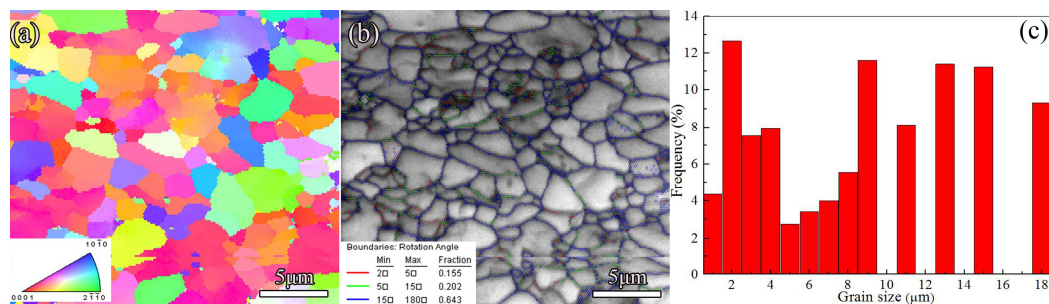


Figure 5. EBSD analyses of the matrix microstructure within the composite pancake: (a) IPF (inverse pole figure) map; (b) grain boundary map and (c) grain size distribution.

3.2. Tensile Properties

The tensile properties of the as-forged $(\text{TiB}_w + \text{TiC}_p)/\text{Ti}$ composite samples taken from different sampling points and tested at various temperatures are listed in Table 1. Generally, $(\alpha + \beta)$ forging effectively improves both the strength and the elongation, as compared with the as cast $(\text{TiB}_w + \text{TiC}_p)/\text{Ti}$ composite [5]. In general, the central area exhibits better tensile properties than those within the peripheral area. For example, at room temperature (RT), the ultimate tensile strength (UTS) and elongation to failure (δ) of the sample taken from peripheral region are 1023.7 MPa and 1.82%, respectively. In the case of high-temperature testing, the difference in the observed properties is only marginal between the samples taken from different locations. For instance, the UTS of the centre area is just 11 MPa higher than that of the peripheral region if tested at $650\ ^\circ\text{C}$. In addition, it is evident that the UTS and elongation of both the peripheral area and the centre area follow the similar trend, i.e., the strength decreases while the elongation increases with temperature.

Table 1. Average tensile properties of 5 vol. % (TiB_w + TiC_p)/Ti composite pancake with different sampling points at room and elevated temperatures.

Sampling Points	25 °C		60 °C		650 °C		700 °C	
	σ_b (MPa)	δ (%)						
near periphery	1023.7	1.82	657.6	5.86	610.9	10.1	493.9	15.3
near centre	1192.1	3.13	701.9	7.78	621.8	14.3	480.5	18.1

3.3. Fracture Morphology

In order to illustrate the fracture characteristics of the 5 vol. % (TiB_w + TiC_p)/Ti composite pancake, tensile fracture surfaces of the centre area are taken as an example. As shown in Figure 6a, the cracked TiB whiskers and TiC particles surrounded by the ductile dimples are observed on the fracture surface. The fracture mode reveals the coexistence of brittle fracture and ductile fracture. It is evident that TiB whiskers and TiC particles embrittle the matrix, with the plastic deformation being very small. In addition, particle pull-out is seldom found on the fracture surface, indicating the good interfacial bonding between the reinforcements and matrix, when the sample is tested at room temperature. As the tensile temperature increases to 600 °C and 650 °C, no obvious changes can be noticed except more and deeper dimples in the matrix, as shown in Figure 6b,c. Therefore, there is no significant change in the fracture mechanism of the (TiB_w + TiC_p)/Ti composite when tested at room temperature to 650 °C. However, upon further increasing the temperature to 700 °C, there exist distinct features on the fracture surface compared to those found below 700 °C. It can be observed in Figure 6d that the dimples dominate the fracture surfaces, indicating the ductile failure at 700 °C. In addition, the pull-outs of TiB whiskers and TiC particles are seen in Figure 6d, implying that interfacial strength decreases and TiC particles detach from the matrix at the interface at 700 °C.

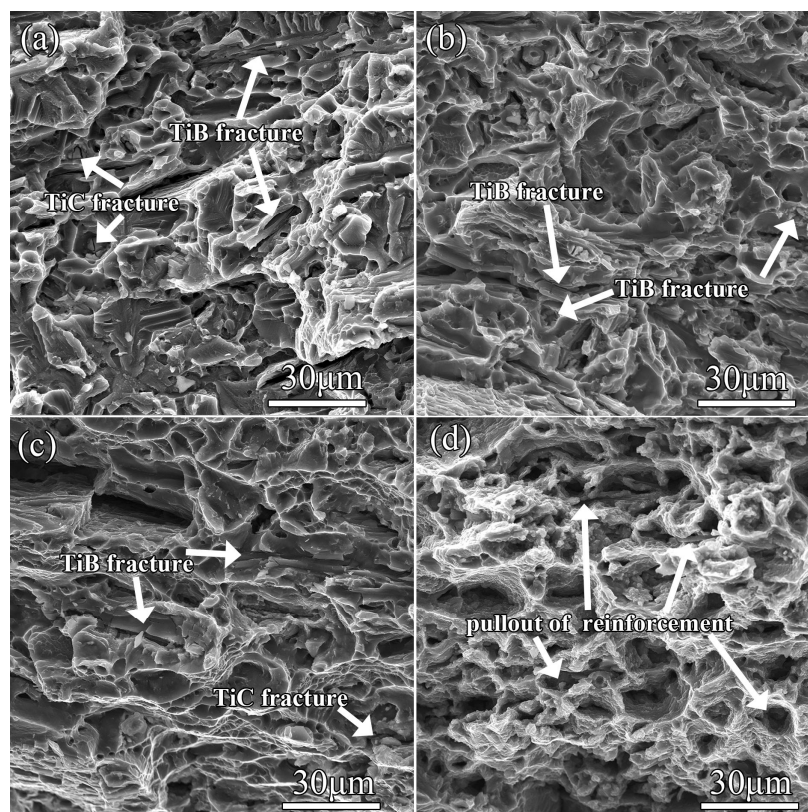


Figure 6. Fracture surfaces of as-forged 5 vol. % (TiB_w + TiC_p)/Ti composite taken in the centre area at different temperatures. (a) room temperature; (b) 600 °C; (c) 650 °C; (d) 700 °C.

4. Discussion

4.1. Microstructure

According to the previous literature [22], the overall section of the forged pancake can be divided into non-deformation region, transition deformation region and homogenous region from the peripheral area to the centre area. The microstructure difference among these areas can be mainly ascribed to inhomogeneous plastic flow during forging. Generally, various heat transfer processes lead to the temperature drop in the peripheral area [23]. Meanwhile, the temperature at the centre of the billet can be raised due to the large amount of heat produced during plastic deformation and friction. The heat is not easy to dissipate because titanium has a low thermal conductivity [19]. Consequently, the deformation preferentially proceeds in the centre area of the pancake and plastic flow decreases gradually from the centre to the periphery. Therefore, for the centre area of the $(\text{TiB}_w + \text{TiC}_p)/\text{Ti}$ composite, due to the relatively high deformation degree, the stored energy in the form of dislocation can be high enough to induce dynamic recrystallisation of the matrix microstructure, as shown in Figure 3c,d. In contrast, the peripheral area has a smaller amount of the stored energy and a relatively low temperature. Thus, the matrix microstructure in the peripheral region does not demonstrate recrystallization features.

As mentioned in Section 3.1, in the peripheral area of the pancake (Figure 3a), the microvoids located at the ends of the reinforcements are observed while no noticeable voids can be found in the centre area (Figure 3d). In fact, due to the different coefficients of thermal expansion between reinforcements and matrix [24], the stress concentration unavoidably generated during forging can exceed the ultimate strengths of the reinforcements, leading to fracture of the reinforcements. Owing to the positive temperature gradient from periphery to centre in the forged pancake, the matrix flow is insufficient to well fill the resulting microvoids at the reinforcements (Figure 3a). While in the centre area, as a result of the relatively high temperature and large deformation, the voids between the reinforcement ends and matrix can be completely closed, as shown in Figure 3d. Similar results were also reported previously [25].

4.2. Tensile Properties

In the current study, the strengths of the centre area within the $(\text{TiB}_w + \text{TiC}_p)/\text{Ti}$ composite pancake are superior to those of the peripheral area. With respect to the strengthening effect, two main factors including grain refinement strengthening and load-carrying capacity of reinforcements, can be considered for the current $(\text{TiB}_w + \text{TiC}_p)/\text{Ti}$ composite [14,15]. According to the classic Hall-Petch theory, the microstructural refinement of matrix can contribute to the improvement in the tensile strength below equi-cohesive temperature [26]. Therefore, strengthening effect caused by grain refinement of the current composite both at room temperature and 600 °C can be discussed together because of that the equicohesive temperature of the matrix alloy within the composite can be regarded as 600 °C [27]. As depicted in Figure 3, the coarse matrix microstructure of the peripheral area (Figure 3a) is gradually refined to equiaxed DRX grains accompanied by the reduction in the size of α grains (Figure 3d). Therefore, the tensile strength of the composite is increased. Additionally, the enhancement in strengths can be partially owing to load-bearing effect arising from TiB_w and TiC_p reinforcements. The micrographs of fracture surfaces presented in Figure 6a,b reveal that most of the TiB_w and TiC_p fracture during tensile test, indicating the interfacial bonding is strong enough to transfer load from matrix to reinforcements. As shown in Figure 3d, the relatively evenly distributed TiB_w and TiC_p shown in the centre area undoubtedly improve the tensile strengths. Therefore, the centre area of the pancake exhibits higher tensile strengths than those within the peripheral area at a temperature from room temperature to 600 °C.

At a temperature above 600 °C, the composite samples still have high strength. This is due to the load-carrying capacity of TiB_w and TiC_p . Boehlert et al. [28] suggested that the load-sharing mechanism requires a good interface bonding between the matrix alloy and the reinforcement. This

has been evidenced in Figure 6c. Ma et al. [29] and Zhang et al. [30] believed that the strengthening effect of reinforcements becomes more profound at high temperatures. In other words, the TiB_w and TiC_p tend to fracture prematurely under stress at low temperatures while the stress around the reinforcements can be released by the ductile matrix at higher temperatures. Therefore, the load transferring effect becomes more remarkable at 650 °C, leading to the superior tensile strength of the centre area within the pancake. As the tensile temperature increases to 700 °C, the prevailing characteristic of interfacial debonding shown in Figure 6d implies that load-carrying of TiB_w and TiC_p ceases. As a result, the centre area exhibits lower strength, as compared with the peripheral region.

5. Conclusions

The following conclusions can be drawn from this study:

1. The as-forged 5 vol. % ($\text{TiB}_w + \text{TiC}_p$)/Ti pancake exhibits inhomogeneous microstructure, with residual transformed β microstructure and microvoids near the randomly distributed TiB_w and TiC_p existing in the peripheral area.
2. The microstructure in the centre area consists of dominant DRX grains plus some refined subgrains and dislocations. The grain size ranges between 1 μm and 7 μm . Moreover, the TiB_w and TiC_p are uniformly distributed within the matrix.
3. Overall, the tensile properties of the composite samples taken from the central area of the pancake are better than those of the samples taken from the peripheral area. Grain refinement strengthening and load-carrying capacity of TiB_w and TiC_p independently or collectively dominate the strengthening mechanism.

Author Contributions: All authors have contributed significantly. C.Z., P.C. and J.H. designed the project. Z.L., J.H., H.Z., S.Z. undertook the experiments and data collection. P.L., Z.L. and C.Z. analysed the data. All authors contributed to the discussion of the results. J.H., C.Z. and P.C. wrote and revised the manuscript.

Funding: This research was funded by the National Natural Science Foundation of China, grant numbers 51504163 and 51604191.

Conflicts of Interest: The authors declare no conflict of interest.

References

1. Huang, L.Q.; Qian, M.; Liu, Z.M.; Nguyen, V.T.; Yang, L.; Wang, L.H.; Zou, J. In situ preparation of TiB nanowires for high-performance Ti metal matrix nanocomposites. *J. Alloys Compd.* **2018**, *735*, 2640–2645. [[CrossRef](#)]
2. Tjong, S.C.; Mai, Y.M. Processing-structure-property aspects of particulate and whisker-reinforced titanium matrix composites. *Compos. Sci. Technol.* **2008**, *68*, 583–601. [[CrossRef](#)]
3. Huang, L.Q.; Wang, L.H.; Qian, M.; Zou, J. High tensile-strength and ductile titanium matrix composites strengthened by TiB nanowires. *Scr. Mater.* **2017**, *141*, 133–137. [[CrossRef](#)]
4. Montealegre-Meléndez, I.; Arévalo, C.; Pérez-Soriano, E.M.; Kitzmantel, M.; Neubauer, E. Microstructural and XRD analysis and study of the properties of the system Ti-TiAl-B4C processed under different operational conditions. *Metals* **2018**, *8*, 367. [[CrossRef](#)]
5. Zhang, C.J.; Kong, F.T.; Xiao, S.L.; Zhao, E.T.; Xu, L.J.; Chen, Y.Y. Evolution of microstructure and tensile properties of in situ titanium matrix composites with volume fraction of (TiB + TiC) reinforcements. *Mater. Sci. Eng. A* **2012**, *548*, 152–160. [[CrossRef](#)]
6. Liu, Y.; Ding, J.; Qu, W.; Su, Y.; Yu, Z. Microstructure Evolution of TiC particles in situ, synthesized by laser cladding. *Materials* **2017**, *10*, 281. [[CrossRef](#)] [[PubMed](#)]
7. Huang, L.J.; Geng, L.; Peng, H.X. In situ ($\text{TiB}_w + \text{TiC}_p$)/Ti6Al4V composites with a network reinforcement distribution. *Mater. Sci. Eng. A* **2010**, *527*, 6723–6727. [[CrossRef](#)]
8. Zhang, W.C.; Wang, M.M.; Chen, W.Z.; Feng, Y.J.; Yu, Y. Preparation of TiB_w /Ti-6Al-4V composite with an inhomogeneous reinforced structure by a canned hot extrusion process. *J. Alloys Compd.* **2016**, *669*, 79–80. [[CrossRef](#)]

9. Li, S.F.; Kondoh, K.; Imai, H.; Chen, B.; Jia, L.; Umeda, J. Microstructure and mechanical properties of P/M titanium matrix composites reinforced by in-situ synthesized TiC-TiB. *Mater. Sci. Eng. A* **2015**, *628*, 75–83. [[CrossRef](#)]
10. Tabrizi, S.G.; Sajjadi, S.A.; Babakhani, A.; Lu, W. Influence of spark plasma sintering and subsequent hot rolling on microstructure and flexural behavior of in-situ TiB and TiC reinforced Ti6Al4V composite. *Mater. Sci. Eng. A* **2015**, *624*, 271–278. [[CrossRef](#)]
11. Sheydaeian, E.; Toyserkani, E. A new approach for fabrication of titanium-titanium boride periodic composite via additive manufacturing and pressureless sintering. *Composites Part B* **2018**, *138*, 140–148. [[CrossRef](#)]
12. Wang, J.; Li, L.; Tan, C.; Liu, H.; Lin, P. Microstructure and tensile properties of TiC_p/Ti6Al4V titanium matrix composites manufactured by laser melting deposition. *J. Mater. Proc. Technol.* **2018**, *252*, 524–536. [[CrossRef](#)]
13. Mu, X.N.; Cai, H.N.; Zhang, H.M.; Fan, Q.B.; Wang, F.C.; Zhang, Z.H.; Ge, Y.X.; Shi, R.; Wu, Y.; Wang, Z.; et al. Uniform dispersion and interface analysis of nickel coated graphene nanoflakes/pure titanium matrix composites. *Carbon* **2018**, *137*, 146–155. [[CrossRef](#)]
14. Zhang, C.J.; Zhang, S.Z.; Lin, P.; Hou, Z.P.; Kong, F.T.; Chen, Y.Y. Thermomechanical processing of (TiB + TiC)/Ti matrix composites and effects on microstructure and tensile properties. *J. Mater. Res.* **2016**, *31*, 1244–1253. [[CrossRef](#)]
15. Chandravanshi, V.K.; Sarkar, R.; Ghosal, P.; Kamat, S.V.; Nandy, T.K. Effect of minor additions of boron on microstructure and mechanical properties of as-cast near α titanium alloy. *Metall. Mater. Trans. A* **2010**, *41*, 936–946. [[CrossRef](#)]
16. Morsi, K.; Patel, V.V. Processing and properties of titanium-titanium boride (TiB_w) matrix composites—A review. *J. Mater. Sci.* **2007**, *42*, 2037–2047. [[CrossRef](#)]
17. Imayev, V.; Gaisin, R.; Gaisina, E.; Imayev, R.; Fecht, H.J.; Pyczak, F. Effect of hot forging on microstructure and tensile properties of Ti-TiB based composites produced by casting. *Mater. Sci. Eng. A* **2014**, *609*, 34–41. [[CrossRef](#)]
18. Bhat, R.B.; Tamirisakandala, S.; Miracle, D.B.; Ravi, V.A. Thermomechanical response of a powder metallurgy Ti-6Al-4V alloy modified with 2.9 pct boron. *Metall. Mater. Trans. A* **2005**, *36*, 845–857.
19. Liu, B.; Li, Y.P.; Matsumoto, H.; Liu, Y.B.; Liu, Y.; Tang, H.P.; Chiba, A. Thermomechanical response of particulate-reinforced powder metallurgy titanium matrix composites—A study using processing map. *Mater. Sci. Eng. A* **2010**, *527*, 4733–4741. [[CrossRef](#)]
20. Huang, D.M.; Wang, H.L.; Chen, X.; Chen, Y.; Guo, H. Influence of forging process on microstructure and mechanical properties of large section Ti-6.5Al-1Mo-1V-2Zr alloy bars. *Trans. Nonferrous Met. Soc. China* **2013**, *23*, 2276–2282. [[CrossRef](#)]
21. Niu, H.Z.; Kong, F.T.; Chen, Y.Y. Microstructure characterization and tensile properties of β phase containing TiAl pancake. *J. Alloys Compd.* **2011**, *509*, 10179–10184. [[CrossRef](#)]
22. Huang, L.J.; Zhang, Y.Z.; Geng, L.; Wang, B.; Ren, W. Hot compression characteristics of TiB_w/Ti6Al4V composites with novel network microstructure using processing maps. *Mater. Sci. Eng. A* **2013**, *580*, 242–249. [[CrossRef](#)]
23. Zhou, W.; Ge, P.; Zhao, Y.Q. Finite element analysis of temperature field in forging process of Ti-1023 alloy. *Hot Work. Technol.* **2009**, *38*, 21–24.
24. Roy, S.; Suwas, S. The influence of temperature and strain rate on the deformation response and microstructural evolution during hot compression of a titanium alloy Ti-6Al-4V-0.1B. *J. Alloys Compd.* **2013**, *548*, 110–125.
25. Srinivasan, R.; Bennett, M.D.; Tamirisakandala, S. Rolling of plates and sheets from as-cast Ti-6Al-4V-0.1B. *J. Mater. Eng. Perform.* **2008**, *18*, 390–398. [[CrossRef](#)]
26. Armstrong, R.; Codd, I.; Douthwaite, R.M.; Petch, N.J. The plastic deformation of polycrystalline aggregates. *Philos. Mag.* **1962**, *7*, 45–58. [[CrossRef](#)]
27. Xiao, L.; Lu, W.J.; Qin, J.N. High-temperature tensile properties of in situ-synthesized titanium matrix composites with strong dependence on strain rates. *J. Mater. Res.* **2008**, *23*, 3066–3074. [[CrossRef](#)]
28. Boehlert, C.J.; Tamirisakandala, S.; Curtin, W.A.; Miracle, D.B. Assessment of in situ TiB whisker tensile strength and optimization of TiB-reinforced titanium alloy design. *Scr. Mater.* **2009**, *61*, 245–248. [[CrossRef](#)]

29. Ma, F.C.; Lu, W.J.; Qin, J.N.; Zhang, D. Strengthening mechanisms of carbon element in in situ TiC/Ti-1100 composites. *J. Mater. Sci.* **2006**, *41*, 5395–5398. [[CrossRef](#)]
30. Zhang, C.J.; Kong, F.T.; Xu, L.J.; Zhao, E.T.; Xiao, S.L.; Chen, Y.Y. Temperature dependence of tensile properties and fracture behavior of as rolled TiB/Ti composite sheet. *Mater. Sci. Eng. A* **2012**, *556*, 962–969. [[CrossRef](#)]



© 2018 by the authors. Licensee MDPI, Basel, Switzerland. This article is an open access article distributed under the terms and conditions of the Creative Commons Attribution (CC BY) license (<http://creativecommons.org/licenses/by/4.0/>).